

Visualizing the dynamics of tuberculosis pathology using molecular imaging

Alvaro A. Ordonez,^{1,2,3} Elizabeth W. Tucker,^{1,2,4} Carolyn J. Anderson,⁵ Claire L. Carter,⁶ Shashank Ganatra,⁷ Deepak Kaushal,⁷ Igor Kramnik,^{8,9} Philana L. Lin,¹⁰ Cressida A. Madigan,¹¹ Susana Mendez,¹² Jianghong Rao,¹³ Rada M. Savic,¹⁴ David M. Tobin,¹⁵ Gerhard Walzl,¹⁶ Robert J. Wilkinson,^{17,18,19} Karen A. Lacourciere,¹² Laura E. Via,²⁰ and Sanjay K. Jain^{1,2,3}

¹Center for Infection and Inflammation Imaging Research, ²Center for Tuberculosis Research, ³Department of Pediatrics, and ⁴Department of Anesthesiology and Critical Care Medicine, Johns Hopkins University School of Medicine, Baltimore, Maryland, USA. ⁵Department of Chemistry, University of Missouri, Columbia, Missouri, USA. ⁶Hackensack Meridian Health Center for Discovery and Innovation, Nutley, New Jersey, USA. ⁷Southwest National Primate Research Center, Texas Biomedical Research Institute, San Antonio, Texas, USA. ⁸Pulmonary Center, Department of Medicine, Boston University School of Medicine, Boston, Massachusetts, USA. ⁹National Emerging Infectious Diseases Laboratories, Boston University, Boston, Massachusetts, USA. ¹⁰Children's Hospital of Pittsburgh, University of Pittsburgh School of Medicine, Pittsburgh, Pennsylvania, USA. ¹¹Department of Biological Sciences, UCSD, San Diego, La Jolla, California, USA. ¹²National Institute of Allergy and Infectious Diseases (NIAID), NIH, Rockville, Maryland, USA. ¹³Molecular Imaging Program at Stanford, Department of Radiology and Chemistry, Stanford University, Stanford, California, USA. ¹⁴Department of Bioengineering and Therapeutic Sciences, School of Pharmacy and Medicine, UCSF, San Francisco, California, USA. ¹⁵Department of Molecular Genetics and Microbiology, Duke University, Durham, North Carolina, USA. ¹⁶SAMRC Centre for Tuberculosis Research, DST/NRF Centre of Excellence for Biomedical Tuberculosis Research, Division of Molecular Biology and Human Genetics, Faculty of Medicine and Health Sciences, Department of Biomedical Sciences, Stellenbosch University, Cape Town, South Africa. ¹⁷Department of Infectious Diseases, Imperial College London, London, United Kingdom. ¹⁸Wellcome Centre for Infectious Diseases Research in Africa and Institute of Infectious Disease and Molecular Medicine, University of Cape Town, Cape Town, South Africa. ¹⁹The Francis Crick Institute, London, United Kingdom. ²⁰Tuberculosis Research Section, Laboratory of Clinical Immunology and Microbiology, and Tuberculosis Imaging Program, Division of Intramural Research, NIAID, NIH, Bethesda, Maryland, USA.

Nearly 140 years after Robert Koch discovered *Mycobacterium tuberculosis*, tuberculosis (TB) remains a global threat and a deadly human pathogen. *M. tuberculosis* is notable for complex host-pathogen interactions that lead to poorly understood disease states ranging from latent infection to active disease. Additionally, multiple pathologies with a distinct local milieu (bacterial burden, antibiotic exposure, and host response) can coexist simultaneously within the same subject and change independently over time. Current tools cannot optimally measure these distinct pathologies or the spatiotemporal changes. Next-generation molecular imaging affords unparalleled opportunities to visualize infection by providing holistic, 3D spatial characterization and noninvasive, temporal monitoring within the same subject. This rapidly evolving technology could powerfully augment TB research by advancing fundamental knowledge and accelerating the development of novel diagnostics, biomarkers, and therapeutics.

Introduction

Mycobacterium tuberculosis, the causative agent of tuberculosis (TB), remains a global public health emergency, as it is one of the top ten causes of death worldwide and a leading cause of death from a single infectious agent (1). New biomarkers and shorter treatments are therefore urgently needed to curb the TB epidemic (2). The alarming rise of multidrug-resistant (MDR) and extensively drug-resistant (XDR) TB (3, 4) poses additional challenges to TB treatment and signifies a need to not only expand the TB drug pipeline but also optimize the use of current and new TB drugs. Despite successes in the development of better diagnostic

tools (5) and therapeutics (6), a lack of fundamental knowledge of TB pathogenesis and host-pathogen interaction dynamics hinders the development of innovative new tools, effective vaccines, and strategies for TB elimination (7).

M. tuberculosis is notable for complex interactions with the host, leading to diseased states that range from subclinical infection to active disease and varied pathological lesions, such as necrotic lesions, cavitation, bronchiectasis, fibrosis, and pneumonia. These pathologies often coexist simultaneously in the same patient, each with distinct local milieu (bacterial burden, antimicrobial exposure, host response; refs. 8–13). Studies in animal models and TB patients have demonstrated that individual TB lesions within the same host are independent and asynchronous (9, 10, 12, 13). There is also spatial heterogeneity even within the TB lesion, with intralesional differences in bacterial burden and immune response (14–16). Unfortunately, conventional methods, which are primarily based on assays on clinical samples (e.g., sputum, blood, cerebrospinal fluid) or resected tissues, cannot optimally capture the heterogeneity or the temporal changes associated with disease progression or treatment (Figure 1). For instance, clinical samples may not correlate well with the lesion

Authorship note: AAO and EWT are co-first authors.

Conflict of interest: AAO and SKJ are investigators on research grants to Johns Hopkins University from T3 Pharmaceuticals AG, Switzerland; Fujirebio Diagnostics, Malvern, Pennsylvania, USA; and NovoBiotic Pharmaceuticals, Cambridge, Massachusetts, USA. AAO and SKJ are coinventors on pending patents US20150250906A1 and USPA 63/071,755, filed by Johns Hopkins University.

Copyright: © 2021, Ordonez et al. This is an open access article published under the terms of the Creative Commons Attribution 4.0 International License.

Reference information: *J Clin Invest.* 2021;131(5):e145107.

<https://doi.org/10.1172/JCI145107>.

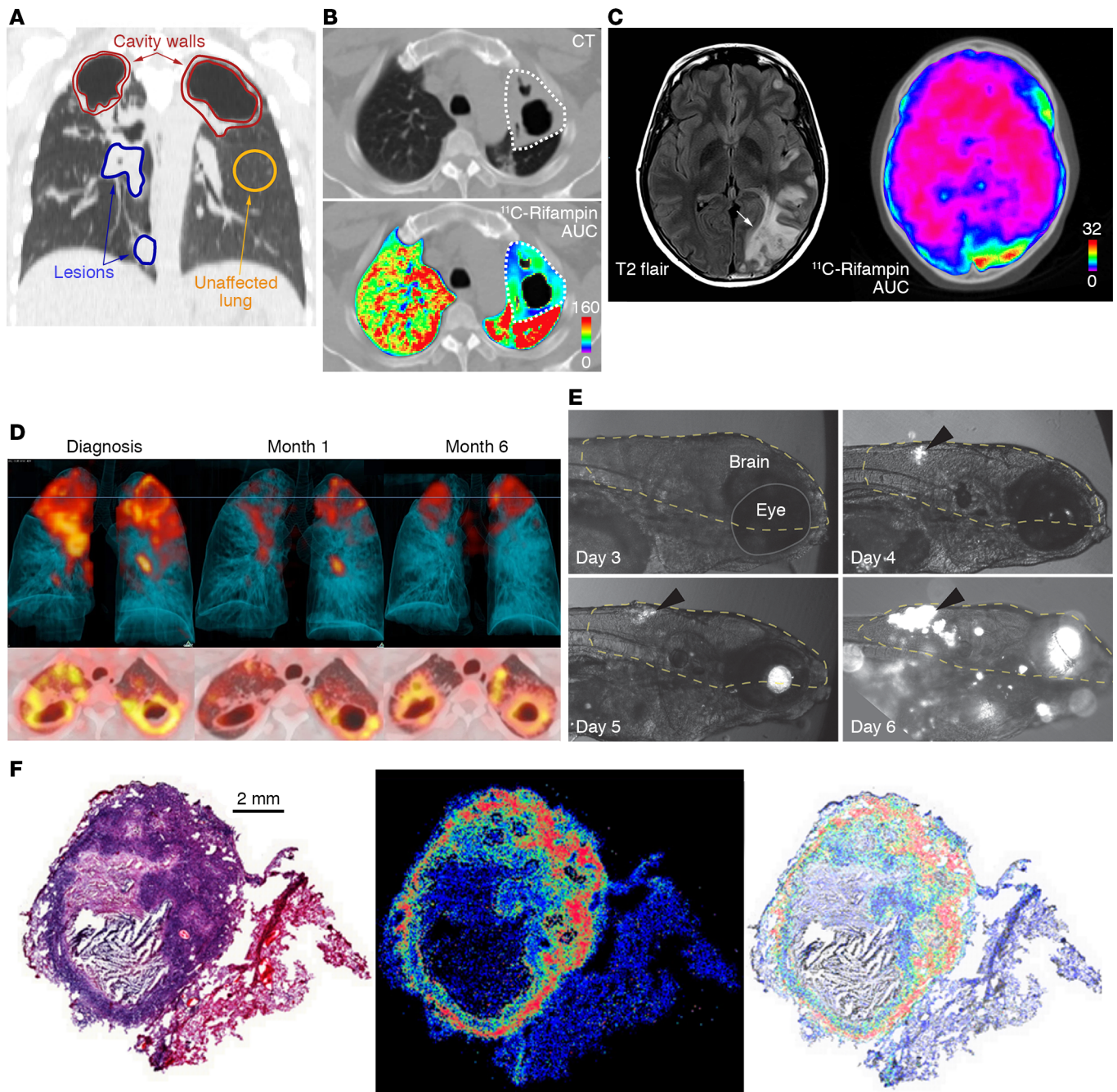


Figure 1. Spatial and temporal heterogeneity in TB lesions. (A) Coronal CT section from a TB patient with newly diagnosed cavitary TB demonstrating pathologically distinct TB lesions – granulomas (blue), pneumonia-like disease (blue), or cavities (red) – compared with unaffected lung (yellow). These different lesions demonstrate distinct pathological characteristics. (B) Radiolabeled ^{11}C -rifampin PET/CT demonstrates spatially compartmentalized rifampin exposures in the pathologically distinct TB lesions within the same patient, with low cavity wall rifampin exposures. The ^{11}C -rifampin AUC is shown as a heatmap overlay in the selected transverse section. A and B were adapted with permission from *Nature Medicine* (13). (C) MRI (T2 flair) demonstrates heterogeneous brain inflammation (arrow) in a patient with TB meningitis with the corresponding spatially heterogeneous ^{11}C -rifampin AUC exposures. Adapted with permission from *Science Translational Medicine* (78). (D) Longitudinal ^{18}F -FDG PET/CT in a cavitary TB patient over 6 months of standard treatment. Increased ^{18}F -FDG uptake (compared with month 1) is noted at 6 months into treatment, coincident with treatment failure. D was adapted with permission from *EJNMMI Research* (108). (E) Fluorescence microscopy allows longitudinal imaging of the brain (dashed line) and eye (solid line) of a zebrafish larva infected i.v. with approximately 100 CFU of fluorescent *Mycobacterium marinum*:tdTomato. Infection began in the hindbrain ventricle (arrowheads). (F) Ex vivo H&E staining of a large rabbit necrotic TB granuloma (left), matrix-assisted laser desorption/ionization mass spectrometry imaging (MALDI-MSI) ion map of moxifloxacin in the same section (middle), and coregistration and overlay of moxifloxacin ion image with H&E staining (in grayscale) demonstrating accumulation in macrophage-rich regions (right). Scale bar: 2 mm. Images in F are courtesy of Drs. Landry Blanc and Véronique Dartois.

Table 1. Description of imaging technologies

Technology	Description
Computed tomography (CT)	Relies on differential levels of x-ray attenuation by tissues within the body to produce a 3D anatomic image.
Magnetic resonance imaging (MRI)	Using a powerful magnet and radiofrequency energy, MRI generates 3D anatomic images with high contrast for soft tissue without ionizing radiation.
Low-field MRI	Low-field MRI (0.5 T vs. 1.5 or 3 T for most clinical scanners) can be used for high-quality imaging of the heart and lungs. This technology is currently under development and is not available for clinical use.
MR spectroscopy (MRS)	Imaging of biochemical processes using endogenous molecules (e.g., choline, creatine, lactate) with ¹ H spectroscopy or substances labeled with exogenous nuclei such as ¹³ C and ¹⁹ F. This technique can be performed with most clinical MRI scanners.
Chemical exchange saturation transfer (CEST) contrast MRI	MR contrast technique to image exogenous or endogenous compounds containing either exchangeable protons or exchangeable molecules. It enables imaging of certain compounds at concentrations that are too low to visualize using standard MR imaging.
Positron emission tomography (PET)	Highly sensitive technology to detect molecules labeled with radioactive isotopes that decay via positron emission (e.g., ¹⁸ F, ¹¹ C). The detectors transform the gamma rays into electrical signals that are reconstructed as 3D tomographic images. Dynamic imaging allows temporal (minutes-seconds-hours) characterization of the pharmacokinetics/metabolism of the labeled molecules.
EXPLORER total-body PET	A PET scanner with geometric coverage to encompass the entire body at once. This provides increased sensitivity (×40) that can be used to perform PET scans at extremely low radiation doses, improve the scan speed (potentially in less than a minute), and track labeled molecules for longer periods of time after injection.
Single-photon emission computed tomography (SPECT)	A rotating gamma camera captures the energies from labeled molecules, which decay via the emission of single gamma rays. Most cameras produce 2D images, although some can perform tomographic 3D reconstructions.
Optical imaging	Macroscopic imaging of live animals and tissues with fluorescent or bioluminescent agents. Highly sensitive; but the use of low-energy photons means that the depth of penetration is limited to only a few centimeters.
Multiphoton intravital microscopy (MP-IVM)	Based on the simultaneous absorption of two or more photons with wavelengths in the near-infrared or infrared range. MP-IVM allows visualization at very high resolution with a depth of a few millimeters.
Ex vivo techniques	
Autoradiography	Radioactive molecules detected and quantified at high resolution by exposure of excised tissues to a detection system (e.g., x-ray film, phosphorimaging screen).
Fluorescence microscopy	Genetically encoded fluorescent reporters or fluorescently tagged molecules to visualize cells and tissues with high resolution.
Fluorescence-lifetime imaging microscopy (FLIM)	Measures how long a fluorophore remains in its excited state before returning to the ground state by emitting a fluorescence photon, which are dependent on variations in the molecular microenvironment. FLIM has been used to provide detailed information on ion concentrations, pH, cellular signaling, and other molecular interactions.
Matrix-assisted laser desorption/ionization mass spectrometry imaging (MALDI-MSI)	Visualization of molecules based on mass detection. MALDI-MSI can simultaneously detect multiple compounds and provides high spatial resolution.

biology at infection sites where the pathogen resides. Moreover, because of the difficulties of obtaining direct tissue and the risk of sampling bias due to lesion heterogeneity, data on human lesion biology remain limited. Essentially, TB is a 21st century global health threat; however, the field continues to be reliant on several diagnostic and research tools developed more than 100 years ago. In contrast to conventional methods that use preserved tissue samples (e.g., histology) to obtain molecular information, molecular imaging approaches focus on imaging molecules of interest within living subjects. Therefore, in this Review, we will focus primarily on imaging of intact living subjects (Table 1), while also highlighting the complementary contributions that other ex vivo imaging technologies, such as matrix-assisted laser desorption/ionization mass spectrometry imaging (MALDI-MSI) and autoradiography, have made to the TB field.

Tomographic imaging can evaluate disease processes deep within the body, noninvasively and relatively rapidly, by providing 3D information about the disease and local biology throughout the body, and is less prone to sampling errors (Table 2). CT provides anatomic information and is used extensively in the clinical management of several diseases, including TB. Chest CT is generally considered superior to chest radiography for identifying features consistent

with TB, especially in children (17). Longitudinal CT has been used to monitor the dynamics of cavity formation in animal models (18, 19) as well as TB treatment response in animals and humans (4, 8, 20–23). MRI provides high-resolution and -contrast anatomic imaging and can detect tissue necrosis (an important pathological feature of TB) with high sensitivity (24). Additionally, MRI has advanced capabilities, such as dynamic contrast-enhanced imaging, chemical exchange saturation transfer (CEST) contrast, and MR spectroscopy (MRS), that can detect physiological or metabolic changes without the need of exogenous agents. In animal models, these novel MRI capabilities were able to differentiate sterile inflammation or oncological processes from bacterial infections (25, 26).

Clinically available whole-body molecular imaging modalities also include nuclear medicine tools such as PET or single-photon emission computed tomography (SPECT), which are based on the detection of the energy produced by radioactive compounds administered in micromolar quantities to a patient or subject. These tools can provide unparalleled opportunities for visualizing infections, especially as molecular and metabolic alterations occur earlier than structural changes. The possibility of radiolabeling a very large number of compounds that can then be detected with PET/SPECT leads to a wide range of applications in clinical and preclinical research.

Table 2. Characteristics of imaging tools

Imaging modality	Relative cost	Temporal resolution/Acquisition times	Spatial resolution	Sensitivity	Comments
In vivo tools					
CT	Moderate	Minutes	Preclinical: 5–100 μm Clinical: 0.5–2 mm	-	High resolution ($\leq 1 \mu\text{m}$) with dedicated scanners for postmortem tissues
MRI	High	Minutes to hours	Preclinical: 0.1–100 μm Clinical: 0.5–1.5 mm	μM	High tissue contrast without ionizing radiation; can also detect molecular events often without the need for exogenous contrast agents
PET	High	Seconds to minutes	Preclinical: 1–2 mm Clinical: 4–10 mm	pM	Detection of molecular events with high sensitivity and ability to target a wide range of biological processes
SPECT	Moderate	Minutes	Preclinical: 0.5–2 mm Clinical: 7–15 mm	nM to pM	Similar to PET with the advantage that multiple radiolabeled agents can be simultaneously detected
Optical imaging	Low	Seconds to minutes	0.1–100 μm	fM	Limited depth penetration, and therefore only applicable to small animals (e.g., zebrafish, mice)
Ex vivo tools					
MALDI-MSI	Moderate	-	μm to cm^{A}	-	Can simultaneously detect multiple molecules – drugs, metabolites, lipids, proteins
Autoradiography	Moderate	-	μm to cm^{A}	-	Nondestructive detection of radiolabeled compounds in tissue or whole-body sections

^ACellular resolution can be achieved with dedicated techniques.

These compounds can be synthesized to target specific biochemical processes that can then be detected and quantified (e.g., glucose metabolism with 2-^[18F]fluoro-2-deoxy-D-glucose [^{18F}-FDG] PET). PET- and SPECT-based technologies have augmented early diagnosis, monitoring, and investigation of various diseases (27). For example, ⁶⁸Ga-DOTATATE PET can detect early neuroendocrine tumors with higher accuracy than conventional imaging modalities (28). Similarly, the implementation of prostate-specific membrane antigen-targeted (PSMA-targeted) PET agents has significantly improved the management of prostate cancer (29). While these tools are integral in the management of patients with cancer, molecular imaging is not widely used for infectious disease but has similar potential (30). PET and SPECT, combined with anatomic imaging (CT, MRI), allow noninvasive detection of dynamic biochemical changes in TB disease without altering the system. This allows the possibility of repeated studies in the same subject, providing longitudinal measurements in the same patient, representing a fundamental advantage over traditional tools. These data can then be used to inform mathematical models of disease progression, which represents a major advance for the field that has primarily relied on snapshots to understand TB. Spatial information enables therapeutic monitoring in patients with deep-seated infections for whom clinical samples (e.g., blood) may be noncorrelative to disease severity and biopsy may be risky or impractical.

Optical imaging provides high-resolution (e.g., single-cell resolution) live imaging in small animal models and has provided valuable insights into biological processes (e.g., TB granuloma formation). Ex vivo techniques can also provide detailed visualization of tissues, and MALDI-MSI is being increasingly utilized in TB research to spatially localize endogenous and exogenous molecules within tissue sections (31). MALDI-MSI is label-free and can localize ionized molecules (e.g., drugs, metabolites, lipids,

proteins) and overlay them onto histologically stained sections to enable spatial distribution of each ion of interest with cellular and subcellular resolution (31, 32). MALDI-MSI can also be applied to archived tissue blocks dating back decades (33).

Pathogen-specific molecular imaging

¹⁸F-FDG PET has been extensively used in TB patients and animal models to monitor and characterize disease (8, 20, 34, 35). Immune cells increase the use of glucose as an energy source during metabolic bursts associated with inflammatory responses due to infection, and this change in glucose utilization can be visualized with ¹⁸F-FDG PET with high sensitivity (36). ¹⁸F-FDG PET/CT has been successfully used to assess TB pathogenesis, bacterial dissemination, and disease progression in animal models that mimic different stages of pulmonary TB disease (37, 38). However, as an analog of glucose, ¹⁸F-FDG is unable to differentiate among oncological, inflammatory, and infectious processes. Therefore, pathogen-specific imaging agents are being developed to specifically detect *M. tuberculosis* complex bacteria. Radio-analogs (e.g., *para*-aminobenzoic acid [ref. 39] and trehalose [ref. 40]) that target specific metabolic pathways present in bacteria but absent in mammalian cells provide opportunities for whole-body imaging to detect *M. tuberculosis* (ref. 30; see Table 3 for a summary of molecular imaging agents that have been used for TB). Similarly, enzyme-activated substrate probes, such as those activated by mycobacterial hydrolases and proteases, can also serve as targets to develop pathogen-specific imaging agents (41). The ability to detect and quantify the bacterial burden using *M. tuberculosis*-specific imaging agents with high sensitivity has potential not only to improve diagnostic accuracy but also to allow the development of tools to noninvasively monitor treatment response and prognosticate disease. It should be noted that all whole-body pathogen-spe-

Table 3. Molecular imaging agents evaluated for TB

Agent	Imaging method	Target	Stage	References
Pathogen-specific				
¹¹ C-PABA	PET	Folate synthesis	Human studies	39, 120
2- ¹⁸ F-PABA	PET	Folate synthesis	Preclinical	39, 121
2- ¹⁸ F-Trehalose	PET	Cell wall	Preclinical	40
CDG-3	Optical	BlaC	Preclinical ^A	122
CNIR800/CNIR5	Optical	BlaC	Preclinical	43, 123
CDG-DNB3	Optical	BlaC and DprE1	Preclinical	44
FLASH	Optical	Hip1	Preclinical	46
DMN-, CDG-, and FITC-labeled trehalose	Optical	Cell wall	Preclinical ^A	45, 47, 124
Host response				
¹⁸ F-FDG	PET	Glucose metabolism	Human studies	10, 57, 108
⁶⁴ Cu-ATSM/ ¹⁸ F-FMISO	PET	Hypoxia	Human studies	91, 92
¹⁸ F-NaF	PET	Chronic TB lesions/calcification	Preclinical	125
^{124/125} I-iodo-DPA-713	PET/SPECT	TSPO	Human studies	60, 61, 83, 84
⁶⁴ Cu-LLP2A	PET	VLA-4	Preclinical	86
⁶⁴ Cu-cFLFLF	PET	FPR1	Preclinical	85
¹⁸ F-ICMT-11	PET	Caspase-3/7	Human studies	90
¹²⁵ I-FIAU	SPECT	Genetically modified <i>M. tuberculosis</i>	Preclinical	126
¹²⁵ I-Anti-C3d mAb	SPECT	iC3b and C3d fragments	Preclinical	127
Drug biodistribution				
¹⁸ F-Isonizaid	PET	–	Preclinical	76
¹¹ C-Rifampin	PET	–	Human studies	13, 75, 78
¹⁸ F-Pyrazinamide	PET	–	Preclinical	128
¹⁸ F-Linezolid	PET	–	Preclinical	77
⁷⁶ Br-Bedaquiline	PET	–	Preclinical	74
^{99m} Tc-Ethambutol	SPECT	–	Human studies	129

^AHuman sputum samples have been evaluated with these agents.

cific imaging approaches for *M. tuberculosis* are in early development. Therefore, detailed preclinical validation and subsequent human studies are required before clinical application.

Optical imaging is a complementary approach to PET/SPECT but is limited by the absorption of light within deep tissues (42), and therefore can be applied primarily to small animal research. For example, specific hydrolysis of a novel fluorescence reporter enzyme substrate by β -lactamase (BlaC), which is naturally expressed by *M. tuberculosis*, was used to image *M. tuberculosis* in situ in a mouse model with high sensitivity (43). Membrane-localized mycobacterial enzymes like BlaC, mycolyltransferase, decaprenyl-phosphoryl-ribose 2'-epimerase (DprE1), and trehalose have been targeted to develop fluorogenic probes that can rapidly detect *M. tuberculosis* in sputum samples (44–46) and within macrophages (47). These enzyme-dependent probes can be used for time-lapse and fixed-cell imaging of mycobacteria in microfluidic devices to visualize single-cell biology (48). Finally, fluorescent reporters have been combined with bronchoscopy for specific detection of bacteria in distal human airways and alveoli (49).

Biomarkers for disease stratification and outcomes

Disease heterogeneity has been a major barrier to clinical studies and patient care, as TB patients with different disease states are grouped together to receive the same treatment. For instance,

since the 1970s and 1980s, it has been known that 80%–85% of patients with uncomplicated, drug-susceptible pulmonary TB may be successfully cured after 4 months of therapy (50). However, the current standard of care still requires a 6-month treatment regimen to avoid relapse, which occurs in a small subset of patients whose characteristics are largely unknown and who are therefore not readily identifiable. Although the 2-month sputum culture status is widely used to assess treatment efficacy in clinical trials and for patient care (51), its correlation with the risk of relapse after treatment completion has been disappointing (52), presumably because sputum bacterial burden only represents lesions in free communication with the airway and thus is not reflective of the total pulmonary disease burden. More recently, promising whole-blood transcriptomic signatures have been identified that correlate with the radiological extent of disease (53) and severity of lung inflammation (54), distinguish patients with active TB from latent infection (55), and potentially identify patients at risk for treatment failure (56). In addition to these advances, imaging techniques could serve as important complementary approaches to noninvasively characterize the diseased states (57).

In a small study in adults with MDR-TB utilizing ¹⁸F-FDG PET as a metabolic marker and CT to assess the radiological extent of disease, quantitative changes in computed abnormal volumes on CT or ¹⁸F-FDG uptake at 2 months into treatment were predictive of long-term outcomes in these patients (20).

¹⁸F-FDG PET/CT has also been used to accurately identify TB reactivation risk in animal models and human subjects (8, 23, 58). A prospective, multicenter, randomized phase IIb clinical trial is under way to evaluate whether baseline stratification of disease burden quantified by ¹⁸F-FDG PET/CT and changes in ¹⁸F-FDG PET/CT parameters at 1 month after treatment initiation can identify pulmonary TB patients who can be cured with 4 months of standard treatment (59). Although ¹⁸F-FDG PET is currently under investigation, more specific imaging biomarkers, such as ¹²⁴I-DPA-713 PET (60, 61), and pathogen-specific molecular imaging approaches (39) could also be used to aid patient stratification, monitor response to treatment, and accelerate the development of novel therapeutics.

Antimicrobial biodistribution

Effective treatment of infections depends on achieving adequate antimicrobial concentrations at infection sites, where the pathogen resides (62). However, because of the difficulties of direct tissue sampling, drug pharmacokinetic (PK) and pharmacodynamic (PD) studies have relied on sequential sampling of blood and rarely other fluids (i.e., cerebrospinal fluid or bronchoalveolar lavage) to measure drug levels. TB creates heterogeneous pathology with multiple disease states occurring simultaneously, with potentially different coexisting microenvironments. Inadequate antimicrobial levels at the site of infection are one important contributor to treatment failure and emergence of MDR and XDR strains (15). However, antimicrobial concentrations account for the majority of variance in TB treatment outcomes (failure, relapse, death), which can be abrogated by higher drug levels (63).

Ex vivo techniques such as MALDI-MSI can provide high-resolution 2D ion maps of molecules (e.g., lipids, proteins, etc.) and their metabolites (64). This technology has been used for nearly a decade to assess drug biodistribution in animal models of TB providing valuable data (65). For instance, Prideaux et al. used MALDI-MSI to demonstrate limited penetration of moxifloxacin into necrotic caseum versus higher levels in the surrounding cellular regions (66). Similarly, MALDI-MSI has confirmed that isoniazid rapidly and homogeneously penetrates TB lesions with rapid clearance (67) and identified multiple patterns of drug distribution in lesions (68–71). A major advantage of MALDI-MSI is that multiple molecules, such as drugs and lipids, can be simultaneously detected from the same tissue (72). While extensive MALDI-MSI data are available from animal models, MALDI-MSI relies on tissue resection, which is only performed in patients when it is clinically indicated for disease management. Thus far, intralésional drug levels have been measured only in patients with refractory disease undergoing surgical resection for clinical reasons (66) and thus may not be representative of the vast majority of TB patients (73). Similarly, the acquisition of longitudinal measurements in the same subject is also challenging.

Whereas MALDI-MSI provides high-resolution drug distribution of resected tissue, PET imaging enables dynamic, longitudinal assessment of drug PK, albeit at a lower resolution. Several key and newer TB drugs, including rifampin, pyrazinamide, isoniazid, linezolid, and bedaquiline, have been radiolabeled to provide noninvasive PK data with PET imaging (Table 3 and

refs. 13 and 74–77). PET imaging can directly visualize multiple compartments simultaneously and monitor changes over time, thereby reducing sampling bias. Coregistration of the PET signal with CT or MRI provides anatomic information and localization of the PET signal with disease pathology. By noninvasive repeat acquisitions, PET can also provide AUC measurements (the critical PD parameter for several TB drugs) or detect changes in antimicrobial distribution during treatment or disease progression (13). For instance, longitudinal PET imaging in a rabbit model of TB meningitis demonstrated a significant decrease in ¹¹C-rifampin brain penetration as early as 2 weeks into treatment (78). Ordonez et al. demonstrated lower penetration of ¹¹C-rifampin in cavitory walls, which are associated with a high bacterial burden, compared with other types of TB lesions as well as independent temporal evolution of different TB lesions in the same patient during treatment (13). Ex vivo autoradiography can also be used with other staining techniques, such as immunofluorescence, in animals after PET to provide high-resolution intralésional biodistribution similar to MALDI-MSI (74). Multimodality imaging can also provide valuable information on the interaction of the host response and drug penetration. However, PET imaging is limited by the radiological half-life, which can range from minutes to days, of the isotope used to radiolabel the drug and is unable to distinguish between the radiolabeled drug and its metabolites.

CT characteristics, such as presence or absence of cavitation, have also been used to stratify patients into easy-to-treat and hard-to-treat phenotypes in patient-level pooled analysis of shortened treatment regimens, and incorporation of additional molecular imaging PK data could provide imaging biomarker information (79–81). Together, the integration of data from molecular imaging and ex vivo techniques could build more accurate and sophisticated PK/PD models to optimize antibiotic treatments and improve outcomes in TB patients (82).

Understanding host-pathogen interactions

Imaging-specific host responses could provide important insights into TB pathogenesis and have potential to serve as biomarkers to predict treatment response and accelerate therapeutic development. Importantly, disease outcomes in certain forms of TB, such as TB meningitis, may be more strongly associated with changes in intracerebral inflammation than with bacterial killing, as immunoinflammatory damage is a critical pathological process in this disease (83). Molecular imaging tools could allow noninvasive readouts of neuroinflammation in animal models as well as in human studies (60, 83).

Radiolabeled iodo-DPA-713, a synthetic ligand for the translocator protein (TSPO), is a specific imaging biomarker for microglia/macrophage-associated inflammation and was predictive of treatment efficacy and relapse in an *M. tuberculosis* murine pulmonary infection model (61, 84). In this model, iodo-DPA-713 imaging was found to be superior to ¹⁸F-FDG PET as a marker for treatment response, and an early increase in iodo-DPA-713 activity, but not ¹⁸F-FDG, correlated significantly with the bacterial burden at relapse (61). Additionally, ¹²⁴I-DPA-713 PET imaging in a rabbit model of TB meningitis showed tracer colocalization with tuberculomas, and postmortem immunohistochemical staining confirmed microglial activation

(83). Biodistribution and dosimetry studies demonstrated that ^{124}I -DPA-713 PET was safe and well tolerated in humans with low pulmonary background signal (60). Therefore, ^{124}I -DPA-713 PET is an example of a molecular imaging approach that could be translated to the clinic to monitor TB-associated microglia/macrophage inflammation.

Other PET ligands targeting various immune cells and biological processes (e.g., apoptosis and hypoxia) are also in development. cFLFLF, which targets formyl peptide receptor 1 (FPR1) expressed in neutrophils and some monocytes in peripheral blood, has been evaluated in animal models of TB (85). Similarly, ^{64}Cu -LLP2A, a high-affinity peptidomimetic ligand for very late antigen-4 (VLA-4; also known as $\alpha_4\beta_1$ integrin), has also been evaluated in *M. tuberculosis*-infected macaques, where VLA-4 was found to be expressed primarily by macrophages and T cells, and to a lesser extent by neutrophils and B cells (86). Molecular imaging can also be used to understand TB pathogenesis and host-directed pharmacological interventions. For example, *M. tuberculosis* proliferates in macrophages during the early phase of infection and induces antiapoptotic proteins, leading to necrosis of the infected cells and subsequent tissue destruction (87, 88). In addition to tissue destruction, necrosis also reduces antibiotic penetration and access to immune cells in the infected sites. Therefore, proapoptotic drugs could be used as host-directed therapies that could be noninvasively monitored using caspase-3/7-specific PET agents like ^{18}F -ICMT-11 and ^{18}F -C-SNAT (89, 90). Similarly, hypoxia-targeting imaging agents have been used in TB to evaluate tissue damage and response to treatment (91, 92).

Although the use of molecular imaging in vaccine development is still in its infancy, it holds promise to elucidate mechanistic information, visualize spatiotemporal dynamics of immune responses, and expedite vaccine development. ^{18}F -FDG PET/CT can be used to noninvasively monitor disease progression in animal models after immunization (93). Similarly, molecular imaging with probes that target specific immune cells can provide valuable information to elucidate the spatiotemporal kinetics of immune responses elicited by a vaccine or subsequent challenge by the pathogen (94, 95). Immune cell-specific imaging could provide information on when and where optimal immune responses develop. Molecular imaging could also be used to monitor “vaccine-take,” a successful immune response to the vaccine, in deep-seated sites, such as pulmonary lymph nodes, in animal models as well as human subjects (96). Moreover, this approach could be used to assess vaccine effect on key immune types and inform optimum vaccine dose and administration route. Finally, molecular imaging can also provide data to identify biomarkers of disease characteristics that could be used to select participants for clinical trials or stratify individuals at enrollment of therapeutic or vaccine trials to control for disease heterogeneity.

Optical imaging can provide complementary data when combined with other methods. For example, while CD4^+ T cells must have direct contact with *M. tuberculosis*-infected cells to provide immunological protection, the mechanisms that restrict this process remain poorly understood (97, 98). However, fluorescent microscopy of engineered mycobacterial strains and cells, including fluorescent reporter T cells specific for activation by antigen, in animal models can overcome these limitations to

better evaluate these processes. For instance, the use of bacterial reporter strains allows imaging of the bacteria within thick lung tissue via fluorescence confocal microscopy, and thus allows evaluation of host-pathogen interactions at a single-bacterium level while retaining the intact lung architecture (99). Techniques such as fluorescence-lifetime imaging microscopy (FLIM) allow the simultaneous use of multiple fluorophores in the same tissue to evaluate different pathological processes. Similarly, *Mycobacterium marinum* and *Mycobacterium leprae* can be used in the zebrafish model (100, 101), which, owing to the optical transparency of the larvae, allows direct visualization of granuloma formation. Recently, mature, fully organized zebrafish granulomas have been microdissected and maintained in 3D in vitro cultures, allowing direct visualization of the granuloma and screening of chemical libraries for potential treatments (102, 103). Multiphoton intravital microscopy (MP-IVM) can also provide quantitative live cell imaging with high contrast, specificity, and resolution. Recent developments have allowed imaging of 1–2 mm of lung tissue surface of live animals using an intercostal window (104) that could allow longitudinal tracking of granulomas located on the lung surface in live *M. tuberculosis*-infected mice (105).

Finally, ex vivo techniques such as MALDI-MSI have been used to interrogate inflammatory signaling lipids within TB lesions, which have been shown to be spatially organized within the developing granuloma (12). Elucidation of this information is critical to understanding host-pathogen interactions during infection, and spatial organization of TB lesions is currently being investigated. Similarly, CT and MRI performed on ex vivo tissues have provided insights into TB pathogenesis, including the characterization of excised human TB tissues (106). Multimodality imaging, such as PET/SPECT and CT/MRI, could be combined with other readouts, such as optical imaging and MALDI-MSI, in preclinical models and select clinical scenarios to provide new insights into host-pathogen interactions.

Implementing molecular imaging: the not-too-distant future

Many molecular imaging techniques can be implemented across multiple animal species as well as for human research (Figure 2). A major advantage of imaging is the ability to follow subjects longitudinally, which can decrease variability and sampling bias, and, for animal studies, substantially decrease the number needed. By decreasing animal numbers, imaging may also improve research costs, which could allow for more efficient experiment. Imaging tools could also be used to stratify disease in preclinical models such that animals assigned to each treatment group have comparable disease. The characteristics of commonly used models for TB and the available imaging tool are summarized in Figure 3. Integration of molecular imaging approaches can complement ex vivo technologies to elucidate mechanisms and to develop novel therapeutics.

Molecular imaging can also benefit clinical research. Although not specific for TB, ^{18}F -FDG PET/CT could be used to screen eligible subjects in clinical trials, determine disease heterogeneity to correctly randomize patients between intervention groups, monitor treatment effects, and help predict outcomes (20, 107, 108). However, a standardized methodology to analyze and represent imaging findings

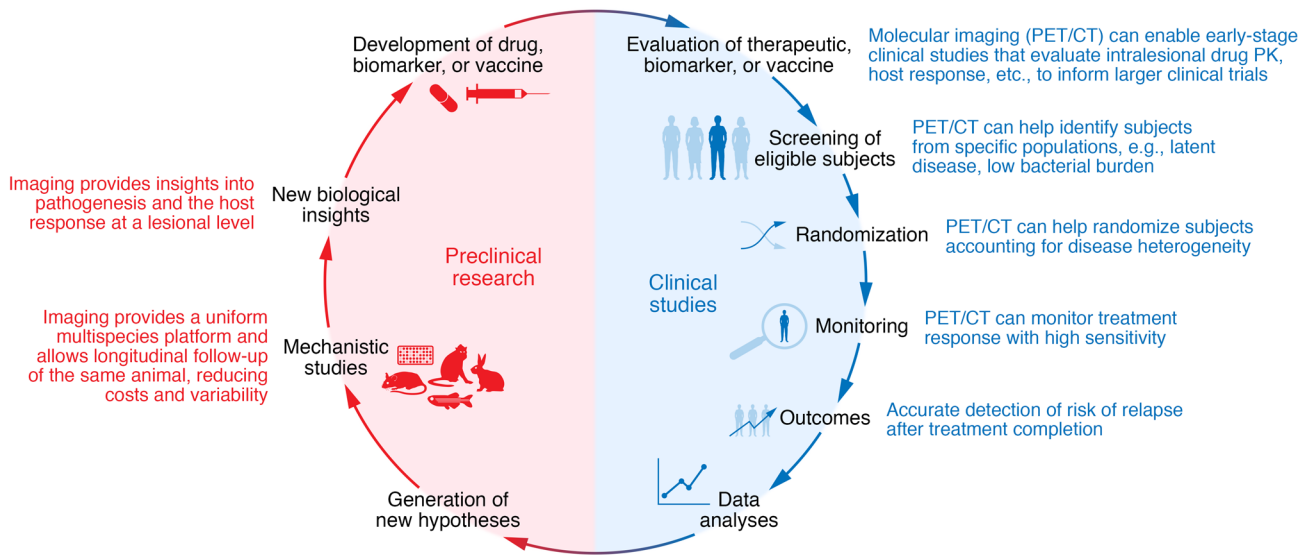


Figure 2. Molecular imaging in the development of new treatments, biomarkers, and vaccines for TB. Molecular imaging can be implemented in the various stages of clinical trials, from early-stage studies to patient screening, randomization, and monitoring of treatment response and outcomes (e.g., relapse), to improve the efficiency and accuracy of TB clinical trials. Additionally, the full spectrum of molecular imaging, including optical imaging and ex vivo techniques, can be employed in preclinical studies. The use of molecular imaging across species allows for crosstalk between preclinical and clinical studies and important collaborative, translational research.

should be implemented to allow accurate comparisons between different studies. Artificial intelligence and machine learning may improve data acquisition, reduce scan times, and improve the speed and accuracy of image interpretations (109, 110). Deep learning algorithms have been used to detect features consistent with pulmonary TB in chest radiographs or CT scans, and it is anticipated that computer-aided tools could streamline image analysis as well as improve reproducibility (17, 111). Furthermore, deep learning algorithms could be used to monitor treatment response by detecting obvious and sub-

tle longitudinal changes in imaging biomarkers. Pathogen-specific PET imaging agents, which are currently in development, could serve as specific diagnostic tools with the potential to provide more accurate data on bacterial burden, and thus provide longitudinal information on infection dynamics and treatment responses (39, 40).

Although advanced molecular imaging tools are not uniformly available in all countries, many developing countries are installing and using advanced imaging tools with increased frequency with imaging studies often performed at a substantially lower cost than







	 In vitro granulomas	 Zebrafish	 Mouse	 Rabbit	 Nonhuman primate	 Human
Necrosis	-	+	+	+	+	+
Cavitation	-	-	+	+	+	+
TB meningitis ^A	-	+	+	+	-	+
Immunological reagents	++	+	++	+	++	++
Availability of transgenic strains	+	++	++	-	-	NA
Cost	+	+	+	++	++++	+++
In vivo imaging tools	Optical imaging		Tomographic imaging (CT, MRI, PET, SPECT)			
Ex vivo imaging tools	MALDI-MSI and autoradiography					

Figure 3. Commonly used TB model systems and their characteristics and utilization in TB imaging research. In vitro granulomas, zebrafish, mice, rabbits, and nonhuman primates are the most common model systems used to recapitulate and study TB. Optical imaging in the zebrafish has been used to study the dynamics of granuloma formation. Mouse and rabbit models have been used to validate multiple imaging tools (PET/SPECT), some of which have been translated into the clinic. ¹⁸F-FDG PET has also been used extensively in nonhuman primate models. ^AAlthough nonhuman primates develop TB meningitis, the characterization of this model has not been reported.

many developed countries (112). Chest CT can be performed rapidly (seconds) with focused PET scans (3–5 minutes) without the need for sedation, even in young children, and with much lower radiation doses owing to improved CT technologies (4, 113). Additionally, many molecular imaging tracers (PET, SPECT) currently under development for TB are rapidly excreted, which substantially decreases radiation exposure.

It should be noted that although patients with MDR-TB have mortality risks similar to or higher than those of patients with many common cancers (112), the use of radiopharmaceutical imaging is accepted for the management of many cancers (even for children) but is avoided for infectious diseases. The advent of higher-resolution, high-sensitivity PET scanners, such as the EXPLORER total-body PET scanner, could increase the use of PET in both pediatric and adult patients with infectious diseases (114–116). MRI does not expose subjects to ionizing radiation but usually requires longer acquisition times. However, more recently, short-sequence lung MRI has been used for pulmonary imaging in TB patients (117). Additionally, low-field-strength (0.5 T) MRI equipped with state-of-the-art hardware can enable the development of lower-cost MRI machines with good image quality in the lung regions (118). Finally, although specialized equipment (cyclotron) is required to synthesize many PET agents, some radionuclides, such as ^{68}Ga , can be synthesized without radionuclide generators and could be produced in remote areas (119). PET agents using ^{18}F (e.g., ^{18}F -FDG) can also be transported locally, usually within a 2- to 3-hour travel radius. By taking these logistics into consideration, a pragmatic approach could allow for more widespread adoption of imaging technologies for TB.

Conclusions

In summary, TB is a 21st-century global health threat; however, the field continues to be reliant on several diagnostic and research tools that were developed more than 100 years ago.

Next-generation molecular imaging is an emerging technology that affords unparalleled opportunities for visualizing infections, as molecular alterations occur earlier than structural changes. The ability for holistic, 3D spatial characterization and noninvasive, longitudinal monitoring in the same subject is a fundamental advantage over current tools and allows detailed insights into the dynamics and spatiotemporal disease heterogeneity noted with TB. Since many molecular imaging tools are readily available for humans, they could advance fundamental knowledge by enabling basic biology studies in TB patients and accelerate the development of new therapeutics, as well as aid clinical management by serving as precision tools for diagnosis, monitoring, and prognostication.

Author contributions

AAO, EWT, and SKJ wrote the initial draft and designed the figures. KAL and SM planned and organized the workshop. All authors participated in the workshop as well as writing and editing the report. The order of co-first authors was determined alphabetically.

Acknowledgments

This Review was inspired by a workshop sponsored by the US National Institute of Allergy and Infectious Diseases on August 26–27, 2019, supported by the Division of Microbiology and Infectious Diseases. We thank all the organizers, speakers, and participants. Logistical support from Mediso USA is also acknowledged. The views expressed in this article are solely those of the authors and do not necessarily represent the official views of the NIH.

Address correspondence to: Sanjay K. Jain, Department of Pediatrics, Johns Hopkins University School of Medicine, 1550 Orleans Street, CRB-II, Room 1.09, Baltimore, MD 21287, USA. Phone: 410.502.8241; Email: sjain5@jhmi.edu.

1. WHO. *Global Tuberculosis Report 2020*. World Health Organization; 2020.
2. Dye C, Williams BG. Eliminating human tuberculosis in the twenty-first century. *J R Soc Interface*. 2008;5(23):653–662.
3. CDC. Emergence of *Mycobacterium tuberculosis* with extensive resistance to second-line drugs—worldwide, 2000–2004. *MMWR Morb Mortal Wkly Rep*. 2006;55(11):301–305.
4. Salazar-Austin N, et al. Extensively drug-resistant tuberculosis in a young child after travel to India. *Lancet Infect Dis*. 2015;15(12):1485–1491.
5. Boehme CC, et al. Rapid molecular detection of tuberculosis and rifampin resistance. *N Engl J Med*. 2010;363(11):1005–1015.
6. Conradie F, et al. Treatment of highly drug-resistant pulmonary tuberculosis. *N Engl J Med*. 2020;382(10):893–902.
7. The NIAID Tuberculosis Research Strategic Plan Working Group. *NIAID Strategic Plan for Tuberculosis Research*. National Institute of Allergy and Infectious Diseases; 2018.
8. Davis SL, et al. Noninvasive pulmonary [^{18}F]-2-fluoro-deoxy-D-glucose positron emission tomography correlates with bactericidal activity of tuberculosis drug treatment. *Antimicrob Agents Chemother*. 2009;53(11):4879–4884.
9. Lin PL, et al. Sterilization of granulomas is common in active and latent tuberculosis despite within-host variability in bacterial killing. *Nat Med*. 2014;20(1):75–79.
10. Murawski AM, et al. Imaging the evolution of reactivation pulmonary tuberculosis in mice using ^{18}F -FDG PET. *J Nucl Med*. 2014;55(10):1726–1729.
11. Gideon HP, et al. Variability in tuberculosis granuloma T cell responses exists, but a balance of pro- and anti-inflammatory cytokines is associated with sterilization. *PLoS Pathog*. 2015;11(1):e1004603.
12. Marakalala MJ, et al. Inflammatory signaling in human tuberculosis granulomas is spatially organized. *Nat Med*. 2016;22(5):531–538.
13. Ordonez AA, et al. Dynamic imaging in patients with tuberculosis reveals heterogeneous drug exposures in pulmonary lesions. *Nat Med*. 2020;26(4):529–534.
14. Dheda K, et al. Spatial network mapping of pulmonary multidrug-resistant tuberculosis cavities using RNA sequencing. *Am J Respir Crit Care Med*. 2019;200(3):370–380.
15. Dheda K, et al. Drug-penetration gradients associated with acquired drug resistance in patients with tuberculosis. *Am J Respir Crit Care Med*. 2018;198(9):1208–1219.
16. Urbanowski ME, et al. Cavitory tuberculosis: the gateway of disease transmission. *Lancet Infect Dis*. 2020;20(6):e117–e128.
17. Jain SK, et al. Advanced imaging tools for childhood tuberculosis: potential applications and research needs. *Lancet Infect Dis*. 2020;20(11):e289–e297.
18. Ordonez AA, et al. Matrix metalloproteinase inhibition in a murine model of cavitory tuberculosis paradoxically worsens pathology. *J Infect Dis*. 2019;219(4):633–636.
19. Urbanowski ME, et al. Repetitive aerosol exposure promotes cavitory tuberculosis and enables screening for targeted inhibitors of extensive lung destruction. *J Infect Dis*. 2018;218(1):53–63.
20. Chen RY, et al. PET/CT imaging correlates with treatment outcome in patients with multidrug-resistant tuberculosis. *Sci Transl Med*. 2014;6(265):265ra166.
21. Tang SJ, et al. Efficacy and safety of linezolid in the treatment of extensively drug-resistant tuberculosis. *Jpn J Infect Dis*. 2011;64(6):509–512.
22. Yanardag H, et al. Computed tomography and bronchoscopy in endobronchial tuberculosis. *Can Respir J*. 2003;10(8):445–448.

23. Lin PL, et al. PET CT identifies reactivation risk in cynomolgus macaques with latent M. tuberculosis. *PLoS Pathog.* 2016;12(7):e1005739.
24. Peprah KO, et al. Characteristic magnetic resonance imaging low T2 signal intensity of necrotic lung parenchyma in children with pulmonary tuberculosis. *J Thorac Imaging.* 2012;27(3):171–174.
25. Liu J, et al. MRI detection of bacterial brain abscesses and monitoring of antibiotic treatment using bacCEST. *Magn Reson Med.* 2018;80(2):662–671.
26. Goldenberg JM, et al. Differentiation of myositis-induced models of bacterial infection and inflammation with T2-weighted, CEST, and DCE-MRI. *Tomography.* 2019;5(3):283–291.
27. Higgins LJ, Pomper MG. The evolution of imaging in cancer: current state and future challenges. *Semin Oncol.* 2011;38(1):3–15.
28. Sanli Y, et al. Neuroendocrine tumor diagnosis and management: 68Ga-DOTATATE PET/CT. *AJR Am J Roentgenol.* 2018;211(2):267–277.
29. Salas Fragomeni RA, et al. Imaging of nonprostate cancers using PSMA-targeted radiotracers: rationale, current state of the field, and a call to Arms. *J Nucl Med.* 2018;59(6):871–877.
30. Ordonez AA, et al. Molecular imaging of bacterial infections: overcoming the barriers to clinical translation. *Sci Transl Med.* 2019;11(508):eaax8251.
31. Blanc L, et al. Visualization of mycobacterial biomarkers and tuberculosis drugs in infected tissue by MALDI-MS imaging. *Anal Chem.* 2018;90(10):6275–6282.
32. Niehaus M, et al. Transmission-mode MALDI-2 mass spectrometry imaging of cells and tissues at subcellular resolution. *Nat Methods.* 2019;16(9):925–931.
33. Paine MRL, et al. Digestion-free analysis of peptides from 30-year-old formalin-fixed, paraffin-embedded tissue by mass spectrometry imaging. *Anal Chem.* 2018;90(15):9272–9280.
34. Ankrah AO, et al. PET/CT imaging of *Mycobacterium tuberculosis* infection. *Clin Transl Imaging.* 2016;4:131–144.
35. Via LE, et al. Infection dynamics and response to chemotherapy in a rabbit model of tuberculosis using [¹⁸F]-12-fluoro-deoxy-D-glucose positron emission tomography and computed tomography. *Antimicrob Agents Chem.* 2012;56(8):4391–4402.
36. Marjanovic S, et al. Expression of glycolytic isoenzymes in activated human peripheral lymphocytes — cell-cycle analysis using flow-cytometry. *Exp Cell Res.* 1991;193(2):425–431.
37. Diedrich CR, et al. SIV and *Mycobacterium tuberculosis* synergy within the granuloma accelerates the reactivation pattern of latent tuberculosis. *PLoS Pathog.* 2020;16(7):e1008413.
38. Coleman MT, et al. Early changes by ¹⁸F-fluoro-deoxyglucose positron emission tomography coregistered with computed tomography predict outcome after *Mycobacterium tuberculosis* infection in cynomolgus macaques. *Infect Immun.* 2014;82(6):2400–2404.
39. Ordonez AA, et al. A systematic approach for developing bacteria-specific imaging tracers. *J Nucl Med.* 2017;58(1):144–150.
40. Pena-Zalvidea S, et al. Chemoenzymatic radio-synthesis of 2-deoxy-2-[¹⁸F]fluoro-D-trehalose ([¹⁸F]-2-FDTre): a PET radioprobe for in vivo tracing of trehalose metabolism. *Carbohydr Res.* 2019;472:16–22.
41. Lentz CS, et al. Design of selective substrates and activity-based probes for hydrolase important for pathogenesis 1 (HIP1) from *Mycobacterium tuberculosis*. *ACS Infect Dis.* 2016;2(11):807–815.
42. Durkee MS, et al. Fluorescence modeling of in vivo optical detection of *Mycobacterium tuberculosis*. *Biomed Opt Express.* 2019;10(10):5445–5460.
43. Yang HJ, et al. Real-time imaging of *Mycobacterium tuberculosis*, using a novel near-infrared fluorescent substrate. *J Infect Dis.* 2017;215(3):405–414.
44. Cheng Y, et al. Rapid and specific labeling of single live *Mycobacterium tuberculosis* with a dual-targeting fluorogenic probe. *Sci Transl Med.* 2018;10(454):eaar4470.
45. Kamariza M, et al. Rapid detection of *Mycobacterium tuberculosis* in sputum with a solvatochromic trehalose probe. *Sci Transl Med.* 2018;10(430):eaam6310.
46. Babin BM, et al. A chemiluminescent protease probe for rapid, sensitive, and inexpensive detection of live *Mycobacterium tuberculosis* [preprint]. <https://doi.org/10.1101/2020.09.14.296772>. Posted on bioRxiv September 14, 2020.
47. Dai T, et al. A fluorogenic trehalose probe for tracking phagocytosed *Mycobacterium tuberculosis*. *J Am Chem Soc.* 2020;142(36):15259–15264.
48. Boot M, et al. Accelerating early antituberculosis drug discovery by creating mycobacterial indicator strains that predict mode of action. *Antimicrob Agents Chemother.* 2018;62(7):e00083-18.
49. Akram AR, et al. In situ identification of Gram-negative bacteria in human lungs using a topical fluorescent peptide targeting lipid A. *Sci Transl Med.* 2018;10(464):eaal0033.
50. [No authors listed]. Clinical trial of six-month four-month regimens of chemotherapy in the treatment of pulmonary tuberculosis: the results up to 30 months. *Tubercle.* 1981;62(2):95–102.
51. Wallis RS, et al. Month 2 culture status and treatment duration as predictors of tuberculosis relapse risk in a meta-regression model. *PLoS One.* 2013;8(8):e71116.
52. Phillips PP, et al. Limited role of culture conversion for decision-making in individual patient care and for advancing novel regimens to confirmatory clinical trials. *BMC Med.* 2016;14:19.
53. Berry MP, et al. An interferon-inducible neutrophil-driven blood transcriptional signature in human tuberculosis. *Nature.* 2010;466(7309):973–977.
54. Gideon HP, et al. Early whole blood transcriptional signatures are associated with severity of lung inflammation in cynomolgus macaques with *Mycobacterium tuberculosis* infection. *J Immunol.* 2016;197(12):4817–4828.
55. Ho J, et al. A transcriptional blood signature distinguishes early tuberculosis disease from latent tuberculosis infection and uninfected individuals in a Vietnamese cohort. *J Infect.* 2020;81(1):72–80.
56. Thompson EG, et al. Host blood RNA signatures predict the outcome of tuberculosis treatment. *Tuberculosis (Edinb).* 2017;107:48–58.
57. Vorster M, et al. Advances in imaging of tuberculosis: the role of ¹⁸F-FDG PET and PET/CT. *Curr Opin Pulm Med.* 2014;20(3):287–293.
58. Esmail H, et al. Characterization of progressive HIV-associated tuberculosis using 2-deoxy-2-[¹⁸F]fluoro-D-glucose positron emission and computed tomography. *Nat Med.* 2016;22(10):1090–1093.
59. Chen RY, et al. Using biomarkers to predict TB treatment duration (Predict TB): a prospective, randomized, noninferiority, treatment shortening clinical trial. *Gates Open Res.* 2017;1:9.
60. Foss CA, et al. Biodistribution and radiation dosimetry of ¹²⁴I-DPA-713, a PET radiotracer for macrophage-associated inflammation. *J Nucl Med.* 2018;59(11):1751–1756.
61. Ordonez AA, et al. Radioiodinated DPA-713 imaging correlates with bactericidal activity of tuberculosis treatments in mice. *Antimicrob Agents Chemother.* 2015;59(1):642–649.
62. Ehrlich P. Address in pathology on chemotherapeutics: scientific principles, methods, and results. *Lancet.* 1913;2(4694):445–451.
63. Pasipanodya JG, et al. Artificial intelligence-derived 3-way concentration-dependent antagonism of gatifloxacin, pyrazinamide, and rifampin during treatment of pulmonary tuberculosis. *Clin Infect Dis.* 2018;67(suppl 3):S284–S292.
64. Dartois V. The path of anti-tuberculosis drugs: from blood to lesions to mycobacterial cells. *Nat Rev Microbiol.* 2014;12(3):159–167.
65. Prideaux B, et al. High-sensitivity MALDI-MRM-MS imaging of moxifloxacin distribution in tuberculosis-infected rabbit lungs and granulomatous lesions. *Anal Chem.* 2011;83(6):2112–2118.
66. Prideaux B, et al. The association between sterilizing activity and drug distribution into tuberculosis lesions. *Nat Med.* 2015;21(10):1223–1227.
67. Manier ML, et al. Reagent precoated targets for rapid in-tissue derivatization of the anti-tuberculosis drug isoniazid followed by MALDI imaging mass spectrometry. *J Am Soc Mass Spectrom.* 2011;22(8):1409–1419.
68. Blanc L, et al. High-resolution mapping of fluorquinolones in TB rabbit lesions reveals specific distribution in immune cell types. *Elife.* 2018;7:e41115.
69. Dutta NK, et al. Statin adjunctive therapy shortens the duration of TB treatment in mice. *J Antimicrob Chemother.* 2016;71(6):1570–1577.
70. Irwin SM, et al. Bedaquiline and pyrazinamide treatment responses are affected by pulmonary lesion heterogeneity in *Mycobacterium tuberculosis* infected C3HeB/FeJ mice. *ACS Infect Dis.* 2016;2(4):251–267.
71. Prideaux B, et al. Mass spectrometry imaging of levofloxacin distribution in TB-infected pulmonary lesions by MALDI-MSI and continuous liquid microjunction surface sampling. *Int J Mass Spectrom.* 2015;377:699–708.
72. Carter CL, et al. Lipidomic dysregulation within the lung parenchyma following whole-thorax lung irradiation: markers of injury, inflammation and fibrosis detected by MALDI-MSI. *Sci Rep.* 2017;7(1):10343.
73. Hunter RL. The pathogenesis of tuberculosis: the early infiltrate of post-primary (adult pulmonary) tuberculosis: a distinct disease entity. *Front Immunol.* 2018;9:2108.
74. Ordonez AA, et al. Radiosynthesis and PET bioimaging of ⁷⁶Br-bedaquiline in a murine model of tuberculosis. *ACS Infect Dis.* 2019;5(12):1996–2002.

75. DeMarco VP, et al. Determination of ^{11}C rifampin pharmacokinetics within *Mycobacterium tuberculosis*-infected mice by using dynamic positron emission tomography bioimaging. *Antimicrob Agents Chemother*. 2015;59(9):5768–5774.
76. Weinstein EA, et al. Noninvasive determination of 2-[^{18}F]-fluoroisonicotinic acid hydrazide pharmacokinetics by positron emission tomography in *Mycobacterium tuberculosis*-infected mice. *Antimicrob Agents Chemother*. 2012;56(12):6284–6290.
77. Mota F, et al. Radiosynthesis and biodistribution of ^{18}F -linezolid in *Mycobacterium tuberculosis*-infected mice using positron emission tomography. *ACS Infect Dis*. 2020;6(5):916–921.
78. Tucker EW, et al. Noninvasive ^{11}C -rifampin positron emission tomography reveals drug biodistribution in tuberculosis meningitis. *Sci Transl Med*. 2018;10(470):eaau0965.
79. Bartelink IH, et al. New paradigm for translational modeling to predict long-term tuberculosis treatment response. *Clin Transl Sci*. 2017;10(5):366–379.
80. Radtke KK, et al. Alternative dosing guidelines to improve outcomes in childhood tuberculosis: a mathematical modelling study. *Lancet Child Adolesc Health*. 2019;3(9):636–645.
81. Imperial MZ, et al. A patient-level pooled analysis of treatment-shortening regimens for drug-susceptible pulmonary tuberculosis. *Nat Med*. 2018;24(11):1708–1715.
82. Strydom N, et al. Tuberculosis drugs' distribution and emergence of resistance in patient's lung lesions: a mechanistic model and tool for regimen and dose optimization. *PLoS Med*. 2019;16(4):e1002773.
83. Tucker EW, et al. Microglia activation in a pediatric rabbit model of tuberculous meningitis. *Dis Model Mech*. 2016;9(12):1497–1506.
84. Foss CA, et al. Noninvasive molecular imaging of tuberculosis-associated inflammation with radioiodinated DPA-713. *J Infect Dis*. 2013;208(12):2067–2074.
85. Locke LW, et al. Use of a leukocyte-targeted peptide probe as a potential tracer for imaging the tuberculosis granuloma. *Tuberculosis (Edinb)*. 2018;108:201–210.
86. Mattila JT, et al. Positron emission tomography imaging of macaques with tuberculosis identifies temporal changes in granuloma glucose metabolism and integrin $\alpha 4\beta 1$ -expressing immune cells. *J Immunol*. 2017;199(2):806–815.
87. Sly LM, et al. Survival of *Mycobacterium tuberculosis* in host macrophages involves resistance to apoptosis dependent upon induction of antiapoptotic Bcl-2 family member Mcl-1. *J Immunol*. 2003;170(1):430–437.
88. Gan H, et al. *Mycobacterium tuberculosis* blocks crosslinking of annexin-1 and apoptotic envelope formation on infected macrophages to maintain virulence. *Nat Immunol*. 2008;9(10):1189–1197.
89. Palmer M, et al. Preclinical kinetic analysis of the caspase-3/7 PET tracer 18F-C-SNAT: quantifying the changes in blood flow and tumor retention after chemotherapy. *J Nucl Med*. 2015;56(9):1415–1421.
90. Ordonez AA, et al. Caspase-based PET for evaluating pro-apoptotic treatments in a tuberculosis mouse model. *Mol Imaging Biol*. 2020;22(6):1489–1494.
91. Harper J, et al. Mouse model of necrotic tuberculosis granulomas develops hypoxic lesions. *J Infect Dis*. 2012;205(4):595–602.
92. Belton M, et al. Hypoxia and tissue destruction in pulmonary TB. *Thorax*. 2016;71(12):1145–1153.
93. Darrach PA, et al. Prevention of tuberculosis in macaques after intravenous BCG immunization. *Nature*. 2020;577(7788):95–102.
94. Malherbe ST, et al. The potential of imaging tools as correlates of infection and disease for new TB vaccine development. *Semin Immunol*. 2018;39:73–80.
95. Pai M, et al. Tuberculosis. *Nat Rev Dis Primers*. 2016;2:16076.
96. Blazevic A, et al. Pilot studies of a human BCG challenge model. *Tuberculosis (Edinb)*. 2017;105:108–112.
97. Srivastava S, Ernst JD. Cutting edge: direct recognition of infected cells by CD4 T cells is required for control of intracellular *Mycobacterium tuberculosis* in vivo. *J Immunol*. 2013;191(3):1016–1020.
98. Ernst JD, et al. Limited antimycobacterial efficacy of epitope peptide administration despite enhanced antigen-specific CD4 T-cell activation. *J Infect Dis*. 2018;218(10):1653–1662.
99. MacGilvary NJ, Tan S. Fluorescent *Mycobacterium tuberculosis* reporters: illuminating host-pathogen interactions. *Pathog Dis*. 2018;76(3):fty017.
100. Tobin DM, et al. The *lta4h* locus modulates susceptibility to mycobacterial infection in zebrafish and humans. *Cell*. 2010;140(5):717–730.
101. Madigan CA, et al. A macrophage response to mycobacterium leprae phenolic glycolipid initiates nerve damage in leprosy. *Cell*. 2017;170(5):973–985.
102. Cronan MR, et al. An explant technique for high-resolution imaging and manipulation of mycobacterial granulomas. *Nat Methods*. 2018;15(12):1098–1107.
103. Matty MA, et al. Potentiation of P2RX7 as a host-directed strategy for control of mycobacterial infection. *Elife*. 2019;8:e39123.
104. Barlerin D, et al. Biosafety level 3 setup for multiphoton microscopy in vivo. *Sci Rep*. 2017;7(1):571.
105. Entenberg D, et al. A permanent window for the murine lung enables high-resolution imaging of cancer metastasis. *Nat Methods*. 2018;15(1):73–80.
106. Wells G, et al. 3D microarchitecture of the human tuberculosis granuloma [preprint]. <https://doi.org/10.1101/2020.06.14.149898>. Posted on bioRxiv June 15, 2020.
107. Coleman MT, et al. PET/CT imaging reveals a therapeutic response to oxazolidinones in macaques and humans with tuberculosis. *Sci Transl Med*. 2014;6(265):265ra167.
108. Malherbe ST, et al. Quantitative 18F-FDG PET-CT scan characteristics correlate with tuberculosis treatment response. *EJNMMI Res*. 2020;10(1):8.
109. Wahl RL, et al. Mars shot for nuclear medicine, molecular imaging, and molecularly targeted radiopharmaceutical therapy. *J Nucl Med*. 2021;62(1):6–14.
110. LaLonde R, et al. Capsules for biomedical image segmentation. *Med Image Anal*. 2020;68:101889.
111. Khan FA, et al. Chest x-ray analysis with deep learning-based software as a triage test for pulmonary tuberculosis: a prospective study of diagnostic accuracy for culture-confirmed disease. *Lancet Digit Health*. 2020;2(11):e573–e581.
112. Jain SK. The promise of molecular imaging in the study and treatment of infectious diseases. *Mol Imaging Biol*. 2017;19(3):341–347.
113. Andronikou S, et al. Technique, pitfalls, quality, radiation dose and findings of dynamic 4-dimensional computed tomography for airway imaging in infants and children. *Pediatr Radiol*. 2019;49(5):678–686.
114. Cherry SR, et al. Total-body imaging: transforming the role of positron emission tomography. *Sci Transl Med*. 2017;9(381):eaaf6169.
115. Badawi RD, et al. First human imaging studies with the EXPLORER total-body PET scanner. *J Nucl Med*. 2019;60(3):299–303.
116. Lv Y, et al. Mini EXPLORER II: a prototype high-sensitivity PET/CT scanner for companion animal whole body and human brain scanning. *Phys Med Biol*. 2019;64(7):075004.
117. Sodhi KS, et al. Rapid lung MRI in children with pulmonary infections: time to change our diagnostic algorithms. *J Magn Reson Imaging*. 2016;43(5):1196–1206.
118. Campbell-Washburn AE, et al. Opportunities in interventional and diagnostic imaging by using high-performance low-field-strength MRI. *Radiology*. 2019;293(2):384–393.
119. Ebenhan T, et al. Preclinical evaluation of 68Ga-labeled 1,4,7-triazacyclononane-1,4,7-triacetic acid-biotin as a radioligand for PET infection imaging. *J Nucl Med*. 2014;55(2):308–314.
120. Mutch CA, et al. [^{11}C]para-aminobenzoic acid: a positron emission tomography tracer targeting bacteria-specific metabolism. *ACS Infect Dis*. 2018;4(7):1067–1072.
121. Zhang Z, et al. Positron emission tomography imaging with 2-[^{18}F]F-p-aminobenzoic acid detects *Staphylococcus aureus* infections and monitors drug response. *ACS Infect Dis*. 2018;4(11):1635–1644.
122. Sule P, et al. Rapid tuberculosis diagnosis using reporter enzyme fluorescence. *J Clin Microbiol*. 2019;57(12):e01462-19.
123. Kong Y, et al. Imaging tuberculosis with endogenous beta-lactamase reporter enzyme fluorescence in live mice. *Proc Natl Acad Sci U S A*. 2010;107(27):12239–12244.
124. Backus KM, et al. Uptake of unnatural trehalose analogs as a reporter for *Mycobacterium tuberculosis*. *Nat Chem Biol*. 2011;7(4):228–235.
125. Ordonez AA, et al. Imaging chronic tuberculous lesions using sodium [^{18}F]fluoride positron emission tomography in mice. *Mol Imaging Biol*. 2015;17(5):609–614.
126. Davis SL, et al. Bacterial thymidine kinase as a non-invasive imaging reporter for *Mycobacterium tuberculosis* in live animals. *PLoS One*. 2009;4(7):e6297.
127. Foss CA, et al. SPECT/CT imaging of *Mycobacterium tuberculosis* infection with [^{125}I]anti-C3d mAb. *Mol Imaging Biol*. 2019;21(3):473–481.
128. Zhang Z, et al. The biodistribution of 5-[^{18}F] fluoropyrazinamide in *Mycobacterium tuberculosis*-infected mice determined by positron emission tomography. *PLoS One*. 2017;12(2):e0170871.
129. Singh N, Bhatnagar A. Clinical evaluation of efficacy of ^{99m}Tc -ethambutol in tubercular lesion imaging. *Tuberc Res Treat*. 2010;2010:618051.